CHAPTER 8

QUANTIFICATION OF HIGH RESOLUTION PHASE CONTRAST IMAGES THROUGH MULTISLICE IMAGE SIMULATIONS

This chapter describes a method of arriving at quantitative interpretation of lattice images. These are essentially interferograms of direct and diffracted waves from a thin specimen. Interpretation of atomic column contrast images would require nature of single atom potentials of Ag, Au, and Cu atoms as input. This has been generated by a custom written code in Matlab. Following this, the contrast of the experimentally acquired HRTEM images of Ag, Au, Ag-Cu, and Au-Cu NPs oriented along $< 011 >$ have been studied by multislice image simulation with varying defocus and thickness conditions. Interplanar spacings have been compared with the projected structures along $< 011 >$ directions of Au and Ag crystals. In addition, the contrast interpretation and electron channeling behavior through exit wave analyses have been achieved for Au-Cu intermetallic NPs.

8.1 Introduction

The high resolution transmission electron microscopy (HRTEM) is a powerful tool to characterize the nature of atomic arrangements. However, extracting quantitative information from HRTEM is difficult due to several limitations [269]. They arise owing to: (a) weak phase object approximation that cannot be applied to majority of real specimens

(not thin enough); (b) image distortion due to aberrations and instabilities; (c) loss of phase information in the observed electron intensity. Hence, direct match between simulated and experimental images can give misleading results until aforesaid factors are kept in mind during simulation. High resolution phase contrast images need to be interpreted through proper modeling and simulation. The phase and amplitude of the electron wave is modified as it interacts with the specimen potential. The single atom potential for Ag, Au and Cu atom as calculated by Hartree-Fock method is shown in Figure 8.1 [134]. It is observed from the figure that the potential sharply peaks near the nucleus and it falls down asymptotically away from the nucleus. The potential for Ag and Cu are very similar whereas Au exhibits large potential near the nucleus and is different than those of former two. The nature of potential field gets modified depending upon nature of bonding in solids. For ionic compounds as in ceramics, electrons cloud is localized around the nucleus because of which potential field is sharply peaked at the nucleus and dies down very fast away from the nucleus. Potential fields for metals and their alloys as in the present case of NPs of Ag, Au, Ag-Cu and Au-Cu alloys are quite different owing to the presence of free electrons. This adds another level of complication in interpretation of contrast. It has been found in literature that for simple structures image contrast varies in a systematic manner over a range of defocus and thickness [270]. In order to quantitatively understand the contrast and relate it to the atom column position, one has to do simulation and match with the image [271]. To this end, several techniques e.g. multislice simulation, Bloch wave analysis, iterative reconstruction of exit plane wave etc. have been developed. A combination of such techniques has been used successfully for imaging [271–275]. In

the present case, as the atomic positions in cubic Ag, Au, and ordered $AuCu_3$ is known, simulated images could directly be matched with the experimental ones. In this chapter, imaging has been carried out at a predefined defocus value with fixed value of aberration coefficient (C_s = 1.2 mm).

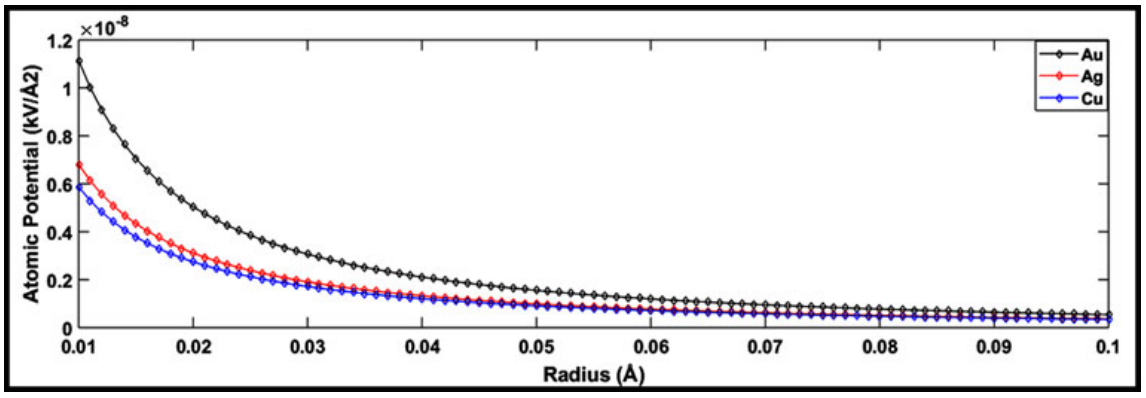

FIGURE 8.1: Calculated single atom potentials of Ag, Au, and Cu.

8.2 Image simulation

As mentioned in the previous section, high resolution images are not directly interpretable and cannot be used for chemical identification of atoms as these images are formed upon interference of the direct electron beam with the diffracted beams. In this process, the phase part is lost in the image plane. The situation becomes complicated as the exit wave function further gets modified by the instrument aberrations. Hence, it is extremely essential to simulate the propagation of the fast electrons inside a specimen which provides insight into the imaging process and helps to interpret the experimental results properly. Careful comparisons between the simulated and the experimental images often reveal the

key structural and chemical information at atomic scale. Image simulations were performed using Java based EMS (JEMS) software developed by P. Stadelmann in this part of the investigation [133]. Multislice simulation has been carried out to simulate cF4 cubic Ag and Au structures as well as cP4 phase of Cu_3Au intermetallic compound. In all these cases, high resolution images have been simulated under varying thickness and defocus conditions along different zone axes through JEMS software. For some of these systems projected potential, exit wave, phase and amplitude part of the exit waves have also been computed with varying thickness. The single atom potentials for elemental Ag, Au and Cu are determined through Hartree-Fock method by solving the parametric equations given by Kirkland (2009) [134]. The cF4 cubic Ag and Au phases have a lattice parameters 0.4086 nm (PDF card no. 01-073-6976) and 0.4078 nm (PDF card no. 00-004-0784) respectively, with their space group $Fm\bar{3}m$. The cF4 phase has fourteen 'a' type positions out of which eight positions have coordinates 000 type and remaining six posses $\frac{1}{2}\frac{1}{2}0$ type respectively. In order to simulate the results, pure Ag and Au lattice has been generated through symmetry operation of the point groups using the crystallographic information available in Pearson's handbook [135]. In a similar way, structures corresponding to the ordered cubic phase of Cu_3Au ($a \sim 0.375$ nm) has also been generated by symmetry operation of the point groups. For all of these structures high resolution images have been simulated under varying thickness and defocus condition by JEMS software [133]. The simulated thickness-defocus maps generated in all the cases are systematically compared with the experimentally recorded high resolution images. The procedure adopted to quantify the high resolution phase contrast images is shown schematically in Figure 8.2. The

HRTEM image of particular nanostructures was recorded at known defocus value. A model atomic arrangements under experimentally observed direction was generated from crystallographic information. Multislice image simulations were performed on model structure and a montage of HRTEM images generated by varying defocus (close to experimental value) and thickness values. Simulated image were matched one by one with that of experimental one. The best match helped in assessing thickness of the specimen.

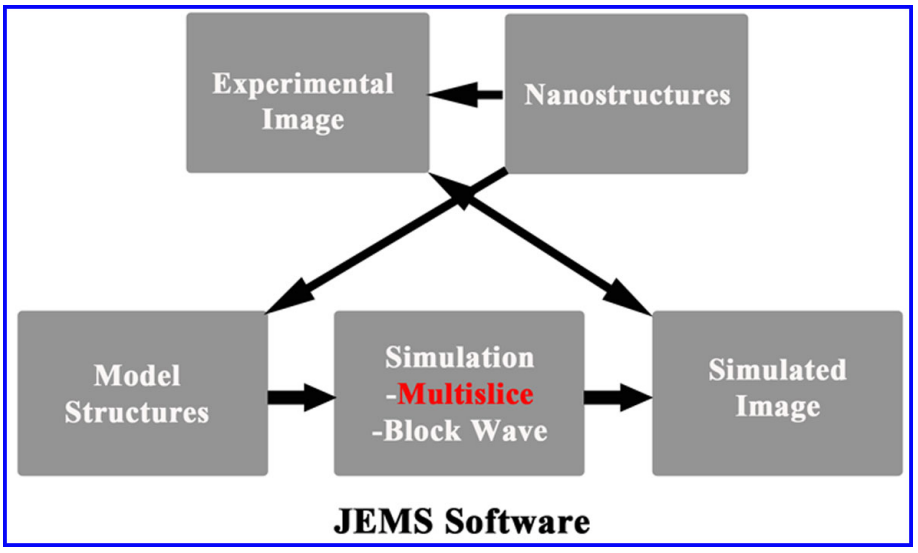

FIGURE 8.2: Schematic of image simulation adopted for quantification of HRTEM images.

8.3 Results and discussion

8.3.1 HRTEM image quantification of Ag NPs

The experimental HRTEM image of Ag NPs along $< 011 >$ zone axis is shown in Figure 8.3 (a) with FFT pattern as inset. The experimental images were captured close to Scherzer defocus which is $\sim$ - 65 nm under 200 kV acceleration voltageand Cs = 1.2 mm.

It is observed that there is a considerable change in contrast with the change in defocus and thickness. The area selected has been chosen for contrast interpretation as shown Figure 8.3 (b). The image consists of bright and dark spots arranged in a periodic manner throughout the particle. These uniform atom columns like contrast suggests that the area under observation is not under strain. In addition, the contrast at the edges appears to be brighter than those at the center of the particle. The appearance of anomalous contrast confirms that the shape of the particle is polyhedral. To quantify the contrast, thickness-defocus maps of Ag crystal oriented along $< 011 >$ are generated in the thickness range from $\sim$ 5 to 8 nm and defocus values from -56 nm to -60 nm as depicted in Figure 8.4. The close match was found for the thickness $\sim$ 7 nm and bright contrast corresponds to Ag atom columns.

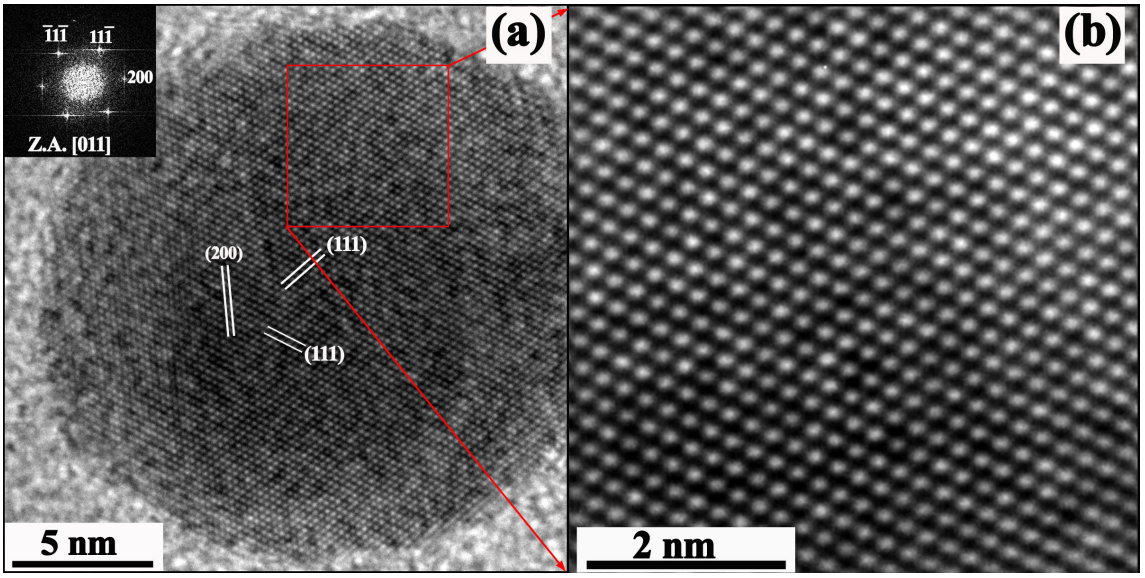

FIGURE 8.3: HRTEM image of Ag NPs acquired along [001] zone axis with FFT as inset (a) and high magnification image selected from (a) for quantification (b).

8.3.2 HRTEM image quantification of AuNPs

The experimental HRTEM image of Au NPs along $< 011 >$ zone axis is shown in Figure 8.5 (a) with FFT pattern as inset. The area selected has been chosen for contrast interpretation as shown Figure 8.5 (b). The contrast consists of bright and dark blobs throughout the particle and is uniform suggests that the area under observation is strain free. In addition, the contrast at the edges appears to be brighter than that of the center of the particle. The appearance of anomalous contrast confirms that the shape of the particle is polyhedral. To quantify the contrast, thickness-defocus maps of Au crystal oriented along $< 011 >$ are

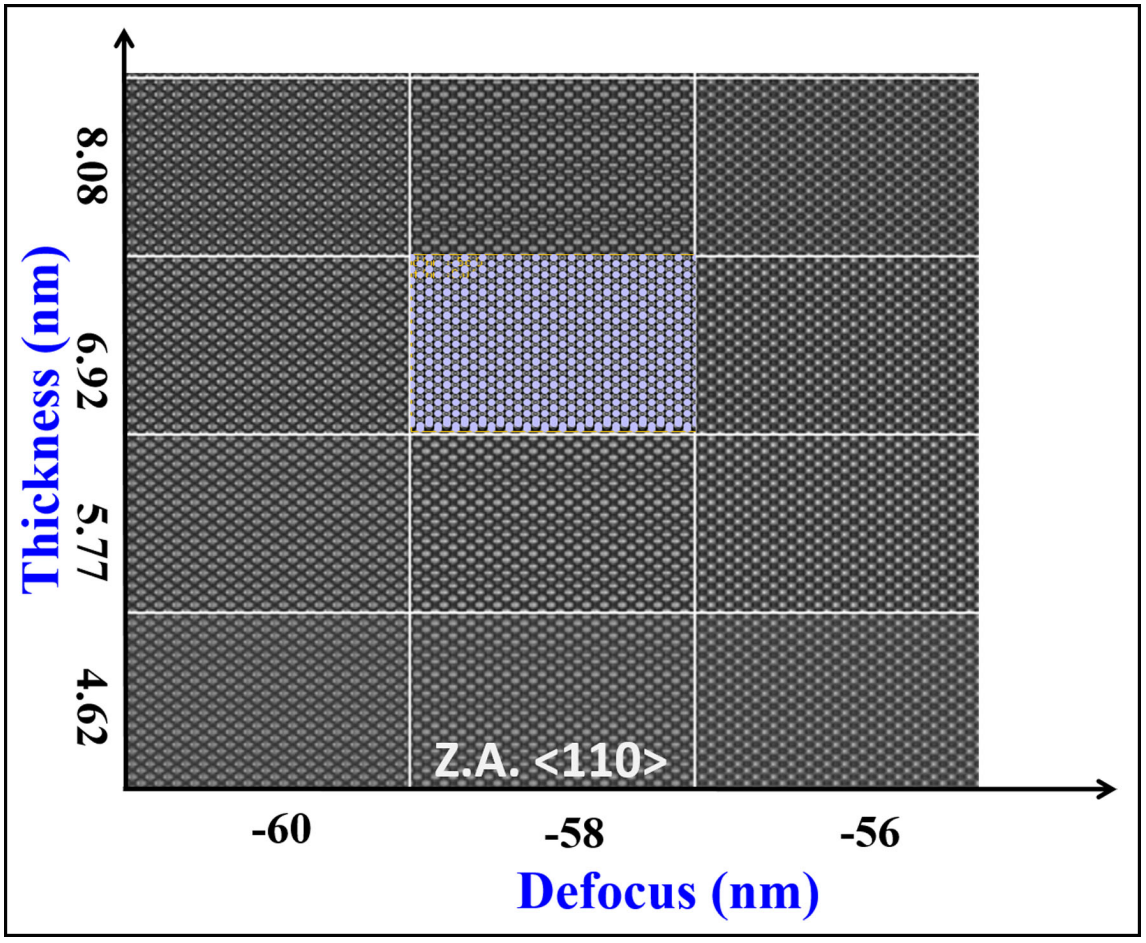

FIGURE 8.4: Simulated images with varying defocus and thickness as well as superimposed Ag atom columns.

generated in the thickness range from $\sim$ 2 to 10 nm and defocus values from -30 nm to -60 nm presented in Figure 8.6. The close match was found for the thickness $\sim$ 8 nm and dark contrast corresponds to Au atom columns.

8.3.3 HRTEM image quantification of Ag-Cu alloy NPs

The experimental HRTEM image of Ag-Cu alloy NPs along $< 011 >$ zone axis is shown in Figure 8.7 (a) with FFT pattern as inset. The contrast consists of bright and dark atoms column like spots throughout the area but with apperarence of difference of background spatially. Additionally, presence of linear contrast is also seen in the experimental image. The appearance of spatial variation in contrast suggests that the area under investigation is not uniform in thickness as defous is fixed. The image simulations performed on pure Ag crystal along $< 011 >$ with varying defocus and thickness condition is shown in Figure 8.7 (b). The simulated images shows complicated contrast patterns by changing

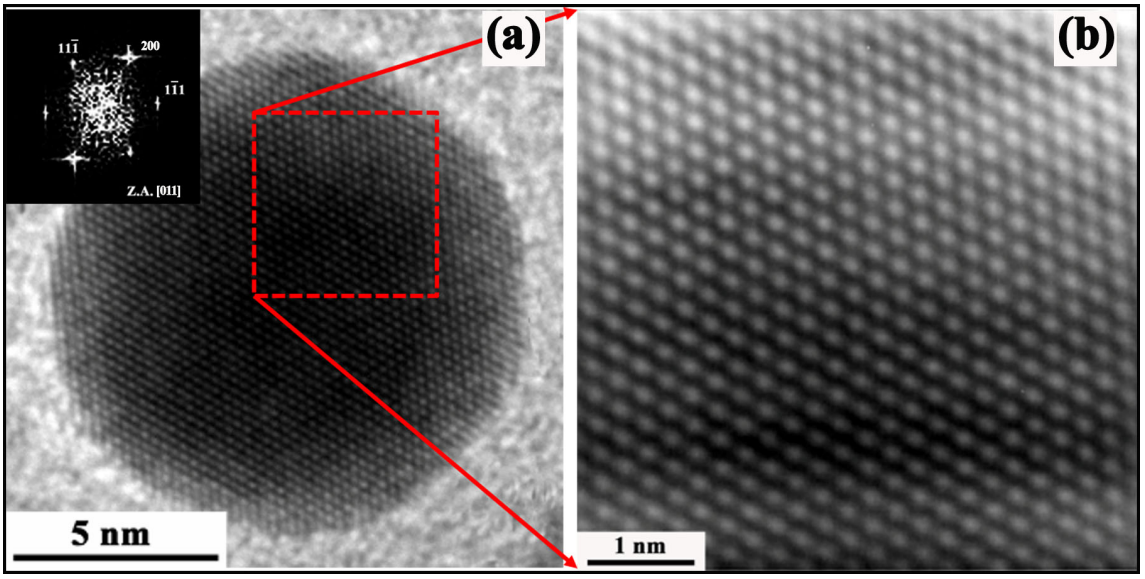

FIGURE 8.5: HRTEM image of Au NPs acquired along [011] with FFT as inset (a) and area selected for quantification (b).

the thickness from $\sim$ 13 to $\sim$ 31 nm and defocus values from -70 nm to -62 nm. The close match was found for the thickness $\sim$ 19 nm and bright dots contrast corresponds to Ag atom columns. However, simulated images at higher thickness values e.g., at $\sim$ 25 nm and 31 nm, matches well with the patterns with linear contrast. This confirms that thickness is not uniform throughout the area under investigation. The shape of the particle therefore,

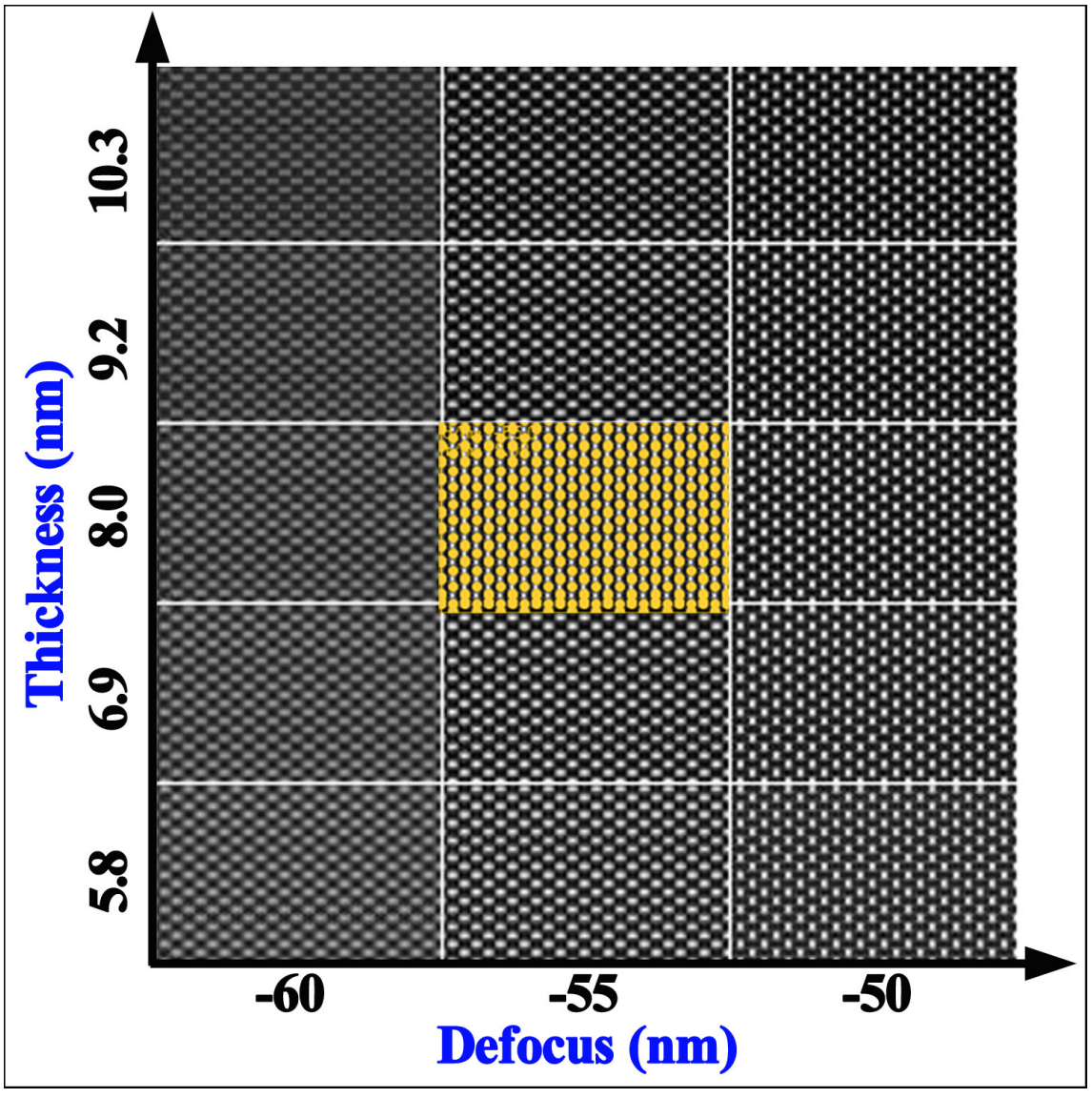

FIGURE 8.6: Simulated images with varying defocus and thickness as well as superimposed Au atom columns.

is polyhedral. The HRTEM image of Ag-Cu alloy NPs and projected structure of pure Ag along $< 011 >$ direction is compared as shown in Figure 8.8 (a) and (b) respectively. The trace of $\{111\}$ and $\{220\}$ planes are shown on the image and they are measured as ~ 0.22,

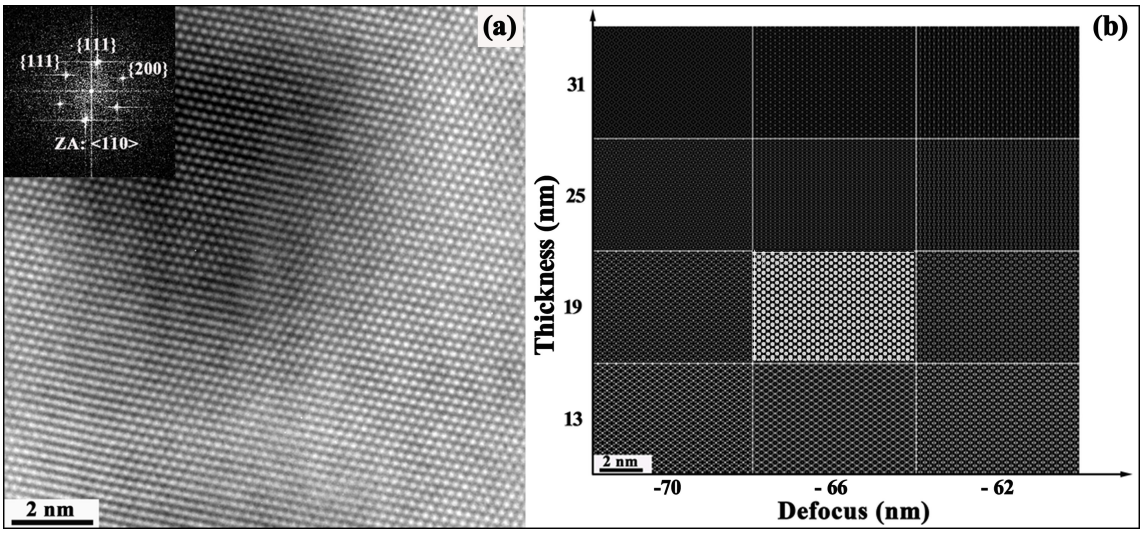

FIGURE 8.7: HRTEM image of Ag-Cu alloy NPs acquired along [011] with FFT as inset (a) and simulated images from pure Ag with varying thickness and defocus (b).

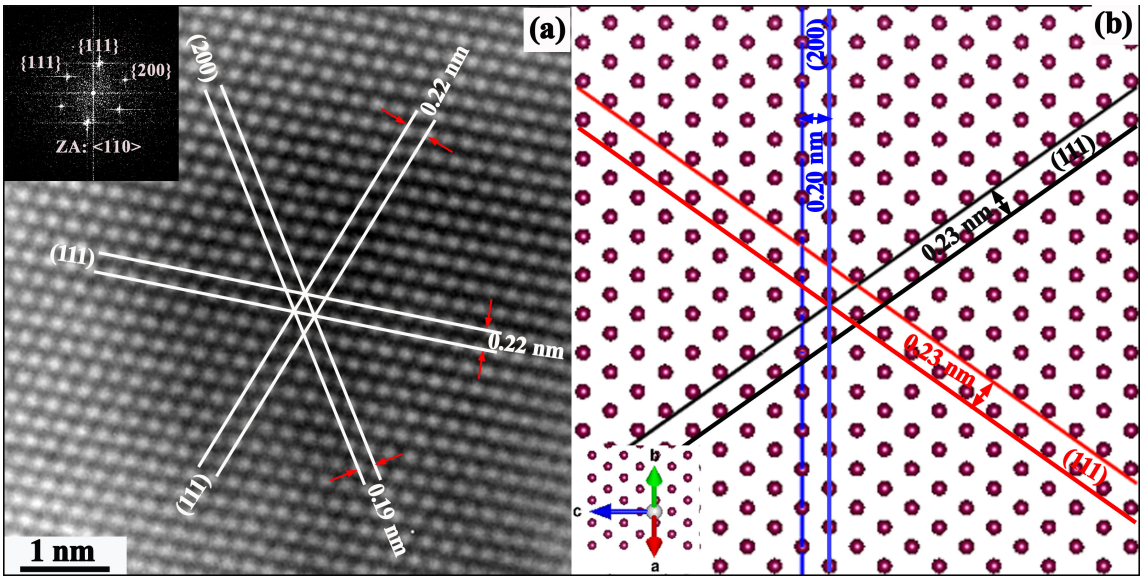

FIGURE 8.8: Experimental image (a) and projected Ag structure along [110] with trace of planes (111) and (200) (b). Lattice planes along with the measured d-spacings are overlaid on the experimental image. Traces of same lattice planes are shown on the projection in (b).

and $\sim$ 0.19 nm, respectively. The deviation from the reported values which are given in Figure 8.8 (b) can be attributed to alloying with Cu. This confirms that solid solubility of Cu in Ag. This has been noted earlier in chapter 4.

8.3.4 HRTEM image quantification of Au-Cu alloy NPs

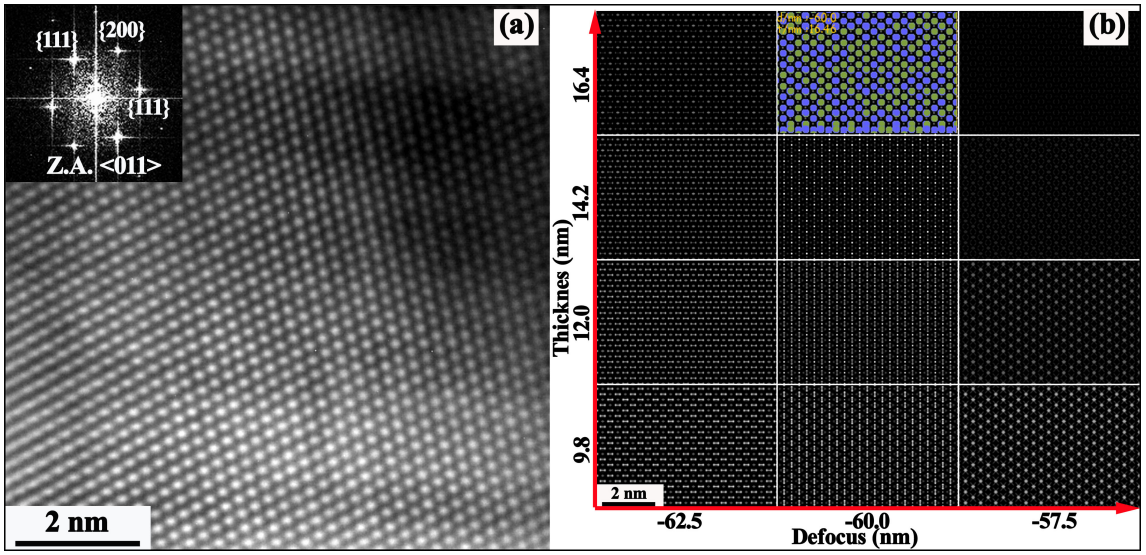

FIGURE 8.9: HRTEM image of Au-Cu alloy NPs acquired along [011] with FFT as inset (a) and simulated images from pure Au with varying thickness and defocus (b).

The experimental HRTEM image of Au-Cu alloy NPs along $< 011 >$ zone axis is shown in Figure 8.9 (a) with FFT pattern as inset. The contrast consists of bright and dark blobs throughout the region though it appears nonuniform suggests that the region under observation may consist of localized strain. In addition, the undulation in contrast can also be seen at different regions. Linear contrast is also noticed in the experimental image. Figure 8.9 (b) shows the thickness-defocus maps of pure Au-Cu alloy crystal oriented along $< 011 >$ are generated in the thickness range from $\sim$ 10 nm to $\sim$ 16 nm and defocus values from -62.5 nm to -57.5 nm. The close match was found for

the thickness $\sim$ 16 nm and dark contrast corresponds to both Au and Cu atom columns. Simulated images at lower thickness values e.g., $\sim$ 10 to 12 nm, matches well with the experimental observation of linear contrast. This suggests that thickness is not uniform throughout the area under investigation. The HRTEM image of Au-Cu alloy NPs and projected structure of pure Au along $< 011 >$ direction is compared as shown in Figure 8.10 (a) and (b) respectively. The trace of $\{111\}$ and $\{220\}$ planes are shown on the image and they are measured as $\sim$ 0.22, $\sim$ 0.23 nm and $\sim$ 0.19 nm, respectively. The deviation from the reported values which are given in Figure 8.10 (b) can be attributed to alloying with Cu.

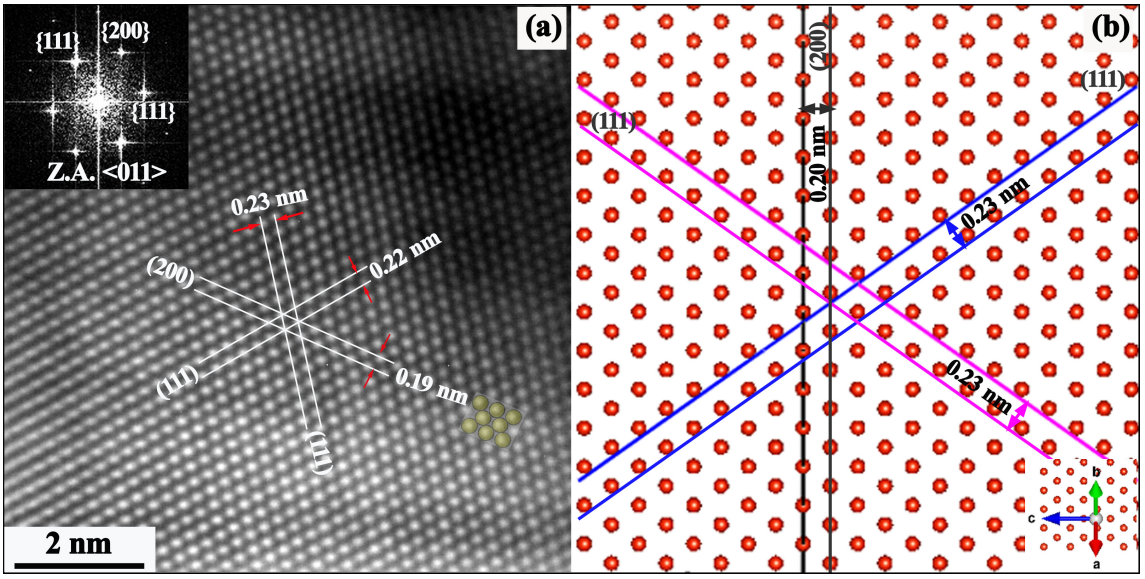

FIGURE 8.10: Experimental image (a) and projected Au structure along [011] with trace of planes 111 and (200) (b).Lattice planes along with the measured d-spacings are overlaid on the experimental image. Traces of same lattice planes are shown on the projection in (b).

8.3.5 Direct structure imaging in Au-Cu intermetallic NPs

The experimental HRTEM image of intermetallic Cu_3Au NPs along [001] zone axis is shown in Figure 8.11(a) with FFT pattern as inset. The image consists of bright and dark dots. The contrast however, varies spatially with appearences of zaggered contrast, assymmetric brigh and dark spots, and linear contrast etc. The area with uniform contrast (bright and dark spots) has been selected (cf. inset in Figure 8.11(a)) for interpretation of contrast such as nature of atom columns and local thickness. Figure 8.11 (b) shows simulated thickness-defocus map of Cu_3Au NPs along [001] zone axis are generated in the thickness range from $\sim$ 24 nm to $\sim$ 32 nm and defocus values from - 82.5 nm to -75 nm. The close match was found for the thickness $\sim$ 30 nm and bright contrast corresponds to Au and front face Cu atom columns. The dark contrast corresponds to other Cu atoms (projected at the edge centres of unit cell) and the representative projected unit

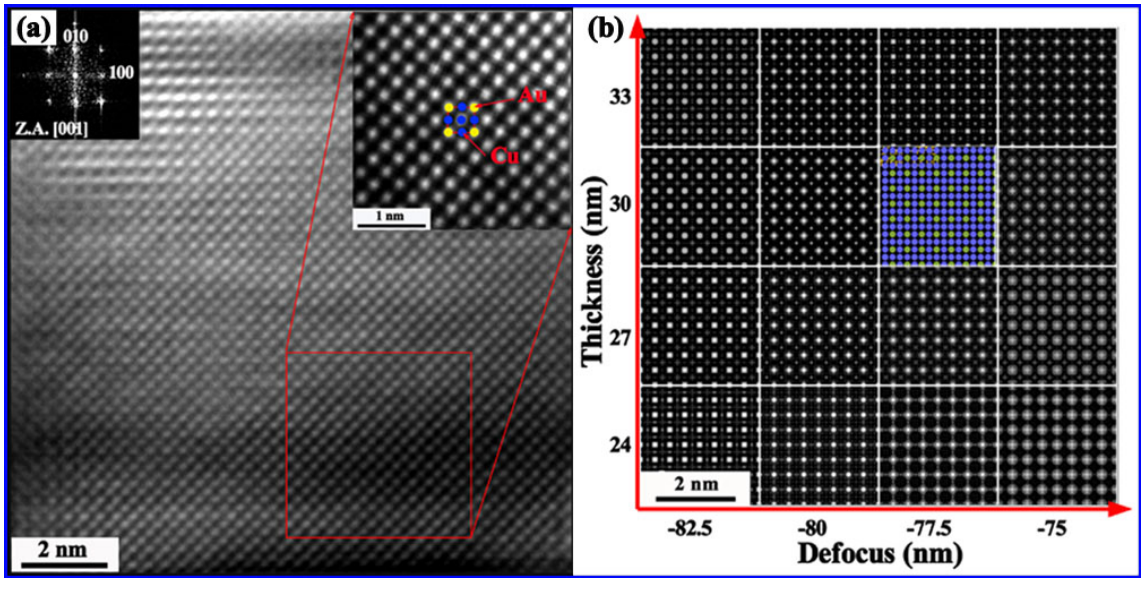

FIGURE 8.11: Experimental HRTEM image of Cu_3Au intermetallic NPs along zone axis [001] (a) and thickness-defocus map of simulated images (b). Insets in (a) shows FFT pattern and area selected for image quantification. Projected unit cell along [001] is also displayed. Atom columns are superimposed in the simulated image.

cell is depicted in Figure 8.11(a). Comparing the experimental and simulated images revealed that all Au and only fron face Cu atom columns have been imaged as bright dots whereas other Cu atoms as dark dots in in the present imaging condition. The alternate bright and dark contrast observed of the Cu atoms can be explained by difference in projected potential encountered by electrons. Figure 8.12 shows the experimental image and corresponding projected structure of Cu_3Au along [001] azimuth. The traces of planes (100) and (110) and corresponding measured planar spacings from experimental image are found to be $\sim$ 0.37 nm and $\sim$ 0.26 nm respectively. A very similar spacings is also measured in simulated image. These findings confirm that region under investigation is strain free.

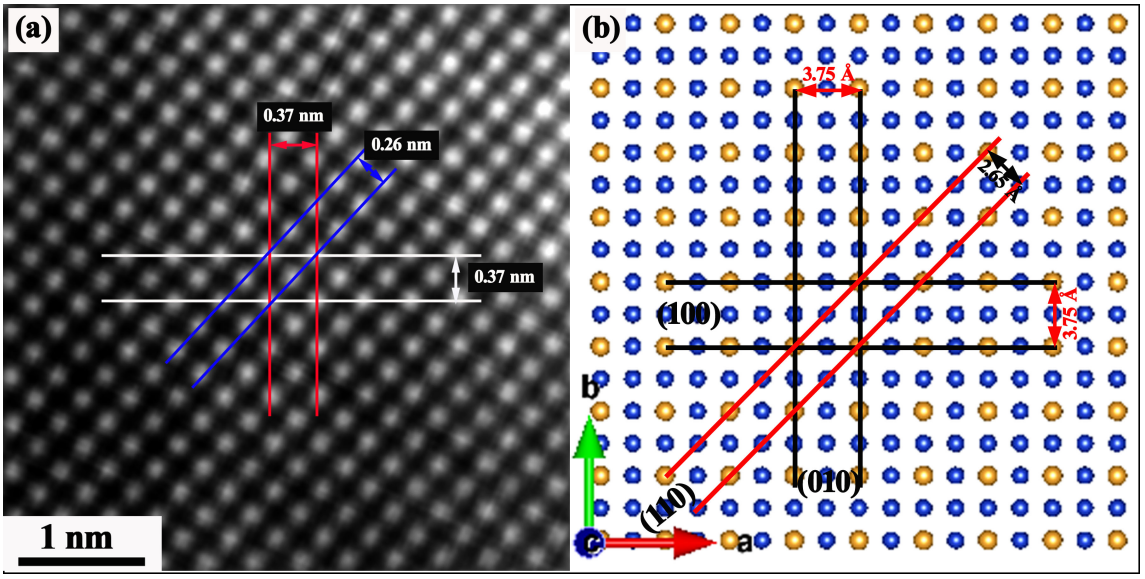

FIGURE 8.12: Experimental HRTEM image along ordered cubic Cu_3Au along [001] zone axis (a) and corresponding projected structure with trace of planes (100), (010), and (110) (b).

8.3.6 Electron channeling behavior along Au and Cu atom columns

The nature of exit wave could be understood qualitatively using image simulation over a thickness range of 6 to 45 nm. Projected potential, exit-plane wave, exit-plane phase and exit-plane amplitude map for cubic Cu_3Au phase are given in Figure 8.13. It is seen from the projected potential map that over a range of thickness, all the atomic columns are present. However, exit-plane wave-phase and amplitude from the Au and the Cu column are quite different (Figure 8.14). It is observed that in the exit-plane wave that comes out of the Au column has nearly invariant phase in the range of thickness (6-45 nm) and the amplitude of the such wave shows little variation with peak at $\sim$ 18 nm. In contrast to that the phase of the exit wave from the Cu columns shows phase reversal after every $\sim$ 9 nm thickness. The exit wave-amplitude from the Cu columns also displays variation over thickness and at higher thicknesses (42-45 nm) they are either very small or absent. The phase reversal of the other face centered Cu atoms projected on the edge of the unit cell has been noticed at thickness of $\sim$ 18 nm. It is clear that the channeling characteristics of electron waves along the Au and Cu columns are different. While the characteristic half length of the electron wave along the Cu column is $\sim$ 9 nm, the same along the Au columns could not be observed in the thickness range of 6 - 45 nm. Preferential imaging of Cu atom columns could be attributed to its potential and the channeling behavior of the electron wave. This helped us assign Cu atom both at the centre of the square net (experimentally seen bright blob and shown as blue for clarity) as well as on the side of the square for which dark blobs are observed experimentally. This is indeed the case when the projected image of Cu_3Au unit cell is seen along [001] direction. Thus, exit wave

analyses may help to understand experimental observation pertaining to Cu occupancy in the unit cell.

8.4 Conclusions

The Multislice image simulations performed with varying thickness and defocus values displayed complicated contrast patterns. Simulated images were matched with the experimental images. The bright and dark dots correspond to Ag and Au atom columns respectively for the Ag and Au samples. The thickness of the quantified regions was found to be $\sim$ 7 nm and 8 nm for Ag and Au NPs respectively. The uniform contrasts across the image could be attributed to strain free regions. The difference in the contrasts at the edges and at the center of the particles was ascribed to the polyhedral shape of the particles. For contrasts interpretation of HRTEM images acquired from Ag-Cu and Au-Cu alloy nanoparticles, it was possible only to identify the heavier atoms like Ag and Au. To understand the alloying behavior and underlying chemistry of AuCu intermetallic NPs, attempts have been made to quantitatively understand the contrast and its interpretation in terms of atom column positions of Au and Cu of high resolution phase contrast images. The close match was found at defocus $\sim$ -80 nm and thickness $\sim$ 30 nm between simulated and experimental image. This comparison allowed to ascertain the chemistry of atom columns individually. The atom columns corresponding to Au and Cu atom columns located at one of the face centered positions could be imaged. This has been understood by invoking concept of atomic potentials. Single atom potential of Au and Cu has been calculated by custom written code in Matlab. Exit wave analysis revealed

the contrast reversal in exit wave phase of Cu atom columns at every $\sim$ 9 nm thickness unlike Au atom columns where phase remained invariant in the entire thickness range (6 to 45 nm). Preferential imaging of Cu atom columns could be understood in the process of such analyses.

FIGURE 8.13: Plot of exit plane wave function, projected potential,wave-phase and wave-amplitude with thickness of ordered cubic Cu_3Au along [001] zone axis.

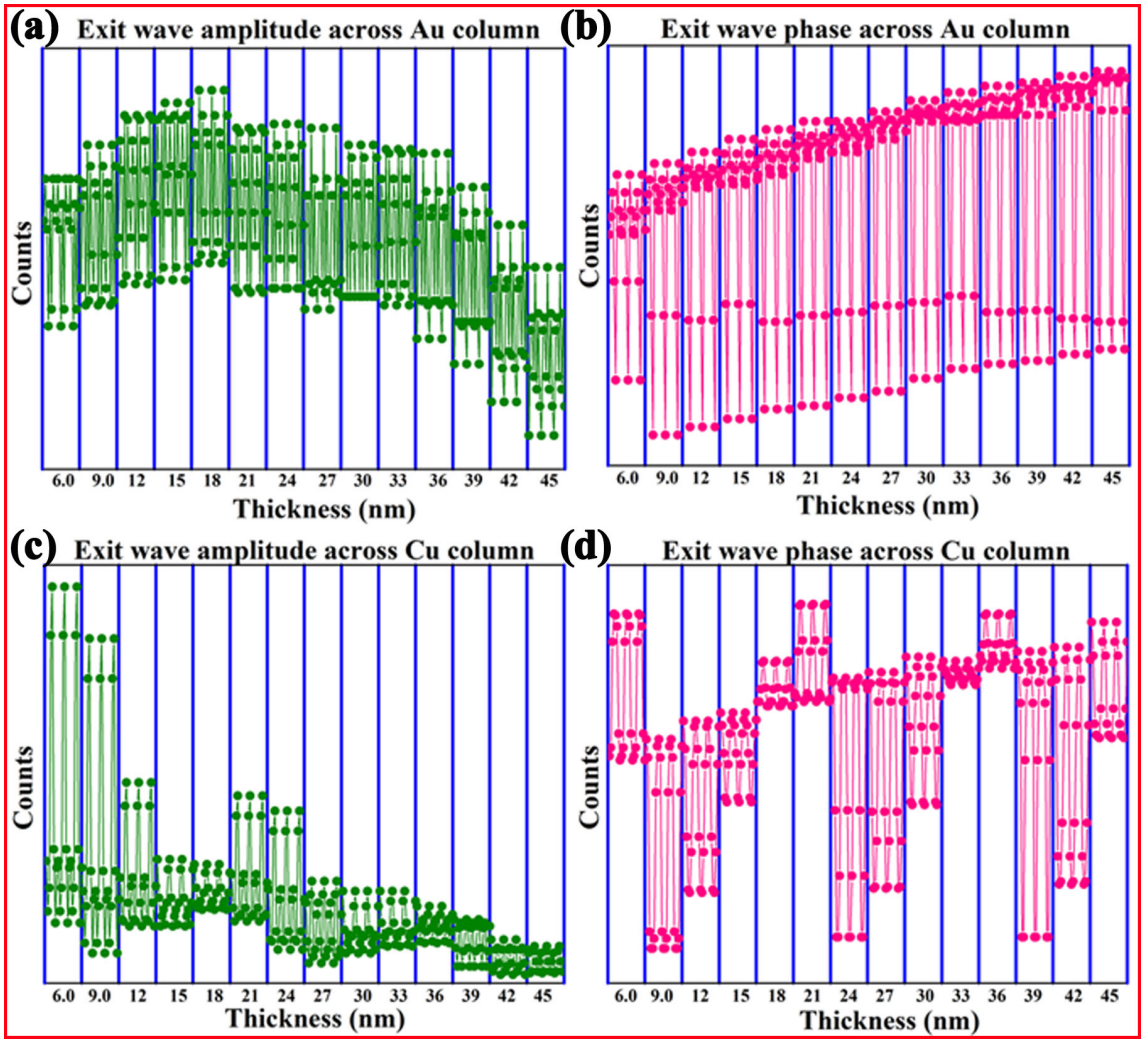

FIGURE 8.14: Variation with thickness of the exit-plane wave amplitude and phase along the Au (a,b) and the Cu (c,d) atom columns in cubic Cu_3Au phase.